International Journal of Nanomedicine

Dovepress
Taylor & Francis Group

Open Access Full Text Article

ORIGINAL RESEARCH

Poly-Lysine-Derived Carbon Quantum Dots Promote the Repair of Bone Defects in Osteomyelitis Through Antibacterial and Osteogenic Effects

Jianghong Wu[1,2,*], He Yan[1,*], Xiaorong Yang[1], Li Qiao[1], Xiancai Rao[2], Renjie Zhou[1]

[1]Department of Emergency, The Second Affiliated Hospital, Army Medical University, Chongqing, People's Republic of China; [2]Department of Microbiology, College of Basic Medical Science, Army Medical University, Chongqing, People's Republic of China

*These authors contributed equally to this work

Correspondence: Xiancai Rao, Department of Microbiology, College of Basic Medical Science, Army Medical University, Chongqing, 400037, People's Republic of China, Email xcrao@tmmu.edu.cn; Renjie Zhou, Department of Emergency, The Second Affiliated Hospital, Army Medical University, Chongqing, 400037, People's Republic of China, Email zhourenjie@tmmu.edu.cn

Background: Osteomyelitis is a challenging clinical condition to manage effectively. In this study, we used ε-Poly (L-lysine) as the raw material to synthesize carbon quantum dots (PL-CQDs). These PL-CQDs possess antibacterial and osteogenesis ability, and are expected to improve the therapeutic effect of osteomyelitis.

Methods: PL-CQDs were synthesized via a dry heat-intermittent ultrasound method and characterized. The antibacterial efficacy of PL-CQDs was assessed using the spread plate method. The biological functions of PL-CQDs were evaluated through CCK-8 assays, scratch wound healing assay, osteogenic differentiation experiments, and transcriptome sequencing. In the in vivo experiments, the rats with osteomyelitis were evenly divided into five groups and treated with calcium sulfate containing different concentrations of PL-CQDs, and the therapeutic effects were evaluated by micro-CT and histology.

Results: PL-CQDs at concentrations of 200, 400, and 800 μg/mL exhibited no cytotoxicity and demonstrated the ability to kill methicillin-resistant *Staphylococcus aureus* and *Escherichia coli*. Additionally, PL-CQDs promoted the migration and osteogenic differentiation of mouse pre-osteoblasts (MC3T3-E1) cells. Transcriptome sequencing revealed that PL-CQDs significantly altered the ECM-receptor interaction signaling pathways and participated in biological processes such as the positive regulation of chondrocyte proliferation, collagen fiber organization, and regulation of fibroblast proliferation. Micro-CT and Masson staining results showed that the incorporation of PL-CQDs at different concentrations was beneficial to the repair of osteomyelitis defects, with the best repair in the PL-CQD50@CS group. Immunohistochemistry (CD31, DMP1) suggested that PL-CQDs facilitated the repair of osteomyelitis by enhancing matrix deposition and vascularization at the bone defect site.

Conclusion: PL-CQDs exhibit antibacterial and osteogenic properties and may serve as a potential alternative treatment for osteomyelitis.

Keywords: carbon quantum dots, osteomyelitis, extracellular matrix deposition

Introduction

Osteomyelitis is an inflammatory bone disease caused by microbial infection, which is characterized by progressive bone destruction and loss. It can be caused by trauma, joint replacement, acute blood-borne infection, etc. *Staphylococcus aureus* (*S. aureus*) is the most common pathogen causing osteomyelitis, accounting for about 75% of the total cases.[1] Research shows the incidence of osteomyelitis in the United States has continued to rise since the 1970s, reaching 24.4 cases per 100,000 people-years.[2] An epidemiological study from China showed that the incidence of post-traumatic osteomyelitis is as high as 2–3%.[3] However, the treatment of osteomyelitis is always challenging, and data suggest that the failure rate of treatment is as high as 10% to 40%.[1] Moreover, the long period and high cost of treatment bring great suffering and heavy financial burden to patients and their families.[4]

Received: 4 March 2025
Accepted: 20 May 2025
Published: 5 June 2025

The application of antibiotics is the key to the treatment of osteomyelitis. Long-term, high-dose, systemic antibiotics application are helpful in infection control,[5] but patients often have poor compliance. In addition, osteomyelitis is often accompanied by severe soft tissue damage, and the formation of scar tissue and sclerotic bone can lead to a decrease in local blood supply. Therefore, despite the concentration of antibiotics in the blood is already high, the concentration at the local lesion remains a cause for concern.[6] Most importantly, this may result in systemic toxicity and the development of drug-resistant bacteria,[7] which complicates the treatment of osteomyelitis. In recent years, the strategy of delivering antibiotics via carrier systems has been employed both experimentally and clinically to treat osteomyelitis, achieving higher antibiotic concentrations at the infection site. However, these carrier systems are mostly made of bioinert materials such as polymethyl methacrylate (PMMA) and poly(lactic-co-glycolic acid) (PLGA), and thus lack bioactivity and osteoinductive capacity. Moreover, while local high concentrations of antibiotics are beneficial for anti-infection, they often produce significant toxicity to the surrounding tissues, thereby interfering with bone regeneration.[8] Therefore, it is urgent to develop new therapeutic strategies for osteomyelitis.

Carbon quantum dots (CQDs) are a type of fluorescent carbon particles with particle size of less than 20 nm. In recent years, these nanoparticles have garnered increasing attention in the field of biomedicine due to their favorable biocompatibility, low toxicity, low cost, and ease of modification.[8,9] Among them, some have demonstrated effective antibacterial properties, which may attributed to their photodynamic and peroxidase-like effects, physical/mechanical damage, disruption of DNA/RNA secondary structure in microorganisms, and inhibition of crucial gene expression.[10–13] In addition, studies have indicated that CQDs can enhance tissue regeneration and have been applied in various biomedical fields, with promising prospects.[14–17] Tang et al prepared nitric oxide-donating CQDs (CQDs-NO) using a two-step hyperthermia-intermittent ultrasonic method and found that CQDs-NO can promote wound vascularization and epithelialization and regulate wound inflammation through the sustained release of NO, thereby facilitating the healing of deep partial-thickness burn wounds.[14] Guo et al synthesized CQDs from *Lycium barbarum* via a hydrothermal strategy, which can alleviate radiation-induced bone injury by inhibiting cellular senescence via regulation of m^5 A modification of *Clip3*.[17] However, the use of CQDs for treating osteomyelitis has rarely been documented.[18,19] This is primarily due to the greater complexity of infection control and bone repair in osteomyelitis compared to the treatment of superficial wounds. Additionally, the preparation of a single CQDs solution is not conducive to its application at osteomyelitis sites. Moreover, the precise effects and mechanisms of CQDs on key cells involved in bone repair, such as mesenchymal stem cells, osteoblasts, and osteoclasts, remain unclear. Calcium sulfate (CS), a widely used bone graft material known for its osteoinductive and bone regenerative properties,[20] is extensively applied in oral surgery, craniofacial surgery, orthopedics, and other fields.[21–23] Furthermore, CS serves as a carrier for local antibiotics and a bone regeneration-promoting material in the treatment of osteomyelitis.[24]

In this study, CQDs with antibacterial properties were synthesized using a dry heat-intermittent ultrasound technique. The effects of these CQDs on mouse pre-osteoblasts cells (MC3T3-E1) and the underlying mechanisms were investigated through experiments on proliferation, migration, differentiation, and transcriptome sequencing. Subsequently, the CQDs were incorporated into CS to develop composite materials for treating osteomyelitis, and their potential application was assessed using rat models.

Materials and Methods

Animals

Male Sprague-Dawley rats, aged 8 weeks and weighing 250–300 g, were obtained from the Experimental Animal Center of Army Medical University in Chongqing, China. The rats were housed at a temperature of 22 ± 1°C, with a relative humidity of 50 ± 1%, and maintained on a 12-hour light/dark cycle. All animal procedures, including euthanasia, were conducted in accordance with the Animal Ethical Statement of Army Medical University (NO.AMUWEC20245231) and complied with the guidelines of the Institutional Animal Care and Use Committee (IACUC).

Reagents

Unless otherwise stated, all reagents were obtained from sigma -Aldrich (St. Louis, MO, USA).

Preparation and Characterization of ε-Poly (L-Lysine) -Derived Carbon Quantum Dots (PL-CQDs)

PL-CQDs were synthesized by a dry heat-intermittent ultrasound method according to the reference[25] with minor modifications. The specific steps are as follows: 1 g of ε-poly (L-lysine) is put into a crucible, heated at 240°C for 3 hours in a muffle furnace, and then natural cooled. The resulting residue was ground into powder and dissolved in 20 mL of deionized water. The mixture was subsequently sonicated for 30 min, centrifuged at 11,000 rpm for 15 min, and dialyzed for 24 h using a dialysis bag with a molecular weight cutoff of 4000 Da. The dialysate was lyophilized and stored at 4°C for future use. The composite material for treating the osteomyelitis model was prepared by mixing PL-CQDs with CS (Osteoset®, [Wright Medical, Memphis, TN, USA]) in varying proportions (specific ratios and assigned names are detailed in Table 1) and cast into a mold. Upon solidification, cylindrical filling materials measuring 3 mm in diameter and 5 mm in height are prepared. The composite materials were immersed in phosphate-buffered saline (PBS, pH 7.4) at 37°C, with the medium being refreshed every 24 hours. Samples were collected on days 2, 4, 6, 8, 10, 12, and 14, respectively. Each sample was rinsed, dried, and weighed to determine the mass loss and degradation rate. The zeta potential of PL-CQDs was measured using a Nano-ZS90 zetasizer (Malvern Instruments, Worcestershire, UK). The morphology and characteristics of PL-CQDs and CS-doped PL-CQDs were analyzed using Transmission Electron Microscopy (TEM) and High-resolution TEM (JEOL-JEM-210 and JEOL-JEM-2100F, respectively, JEOL Ltd., Tokyo, Japan). Fourier Transform Infrared Spectroscopy (FTIR) (NICOLETiS10, Thermo Fisher Scientific, Waltham, MA, United States) was used to investigate the crystal structure and surface functional groups of PL-CQDs. Photoluminescence spectra were recorded using HORIBA Fluoromax-4 (Horiba Scientific, Kyoto, Japan).

Cell Culture

MC3T3-E1 cells were procured from Fu Heng BioLogic Co., Ltd. (Shanghai, China) and cultured in a medium containing 10% (v/v) fetal bovine serum (FBS; [BBI], Boston, MA, USA) and 1% (v/v) penicillin-streptomycin (Solarbio Science & Technology Co., Ltd., Beijing, China). The cells were maintained in a humidified atmosphere with 5% CO_2 at 37°C, with the culture medium refreshed every 2 days.

Cytotoxicity Test

MC3T3-E1 cells were cultured in αMEM medium supplemented with 10%(v/v) FBS at a density of 6000 cells per well in a 96-well plate. After an initial 24-hour culture period, PL-CQDs solution at various final concentrations (0, 200, 400, 800, 1600 μg/mL) was added to the wells, and the cells were cultured for an additional 24 hours. Next, 100 μL of sterile CCK-8 dye (Sevier Biological Technology Co. Ltd., Wuhan, China) was added to each well, and the cells were incubated at 37°C for 1 hour to assess cell proliferation and cytotoxicity. Live and dead cells were distinguished using a live/dead cell double-staining kit (Biyuntian Biotechnology Co., Ltd., Shanghai, China) following the manufacturer's instructions.

Cell Migration Test

The migration ability of MC3T3-E1 cells was assessed using scratch wound healing assay. Briefly, cells were seeded at a density of 5×10^5 cells per well in 6-well plates and cultured overnight. After washing with PBS, a horizontal line was marked on the bottom of the 6-well plate, and the cells were scratched with a 200-μL sterile pipette tip. The cells were gently rinsed twice with PBS to remove the suspended cells and incubated in αMEM medium containing different final concentrations of PL-CQDs (0, 200, 400μg/mL) and 1% (v/v) FBS for 24 hours. Images of scratches were captured at 0

Table 1 Sample Names and Their Respective Components

Group	ddH_2O (mL)	PL-CQDs powder (mg)	CS powder (g)
PL-CQD0@CS	1mL	0	1
PL-CQD5@CS	1mL	0.005	1
PL-CQD50@CS	1mL	0.05	1
PL-CQD500@CS	1mL	0.5	1

https://doi.org/10.2147/IJN.S521727

and 24 hours using an inverted fluorescence microscope (IX73, Olympus, Tokyo, Japan), and the percentage of wound healing was quantified using ImageJ software (version 1.8.0).

Cell Differentiation Assay

Cells were evenly spread on a 6-well plate at a density of 5×10^5 cells per well, and cultured in a constant temperature incubator at 37 °C and 5% CO_2. When the cells were 80 −100% confluent, they were changed to the prepared induction differentiation complete medium. The following combinations of PL-CQDs and CS were added according to the experimental groups: PL-CQDs (0g/mL) + CS (0μg/mL), PL-CQDs (0μg/mL) + CS (0.8μg/mL), PL-CQDs (200μg/mL) + CS (0μg/mL), and PL-CQDs (200μg/mL) + CS (0.8μg/mL). The fresh induction differentiation complete medium and drugs were replaced every 2 days. After 3 weeks of induction, Alizarin red staining was performed according to the instructions of the reagent manufacturer.

Antibacterial Experiment

Single colonies of USA300 (a methicillin-resistant *S. aureus* [MRSA] strain) or DH5α (*Escherichia coli* [*E. coli*]) were picked and inoculated into liquid Brain-Heart Infusion Broth (BHI) or Luria-Bertani (LB) medium, respectively, and cultured overnight at 37°C. The next day, the bacterial suspension was transferred to fresh culture medium at a ratio of 1:100 and culture until they reached the logarithmic growth phase (OD600 between 0.5–1.0). The suspensions were then diluted to 100 times to achieve a bacterial suspension with a concentration of approximately 5×10^7 CFU/mL. A volume of 20μL of PL-CQDs solution with different final concentrations (100, 200, 400, 800μg/mL) were added to 80μL of the bacterial suspension, mixed, and cultured at 37°C for 1 hour. The treated bacterial suspension was diluted 100 -fold, and then 100μL was spread onto the agar plate for colony counting. PBS without LP-CQDs served as the negative control. After treating MRSA and *E. coli* with 800 μg/mL of PL-CQDs for 1 hour, the liquid medium was removed by centrifugation, and the bacteria were washed three times with PBS. Subsequently, the bacteria were fixed with 2.5% glutaraldehyde for 24 hours and then subjected to gradual dehydration. The samples were dried using a critical point drier and sputter-coated with gold. Finally, the morphology of the bacteria was examined using SEM.

Transcriptome Sequencing

MC3T3-E1 cells were seeded at a density of 5×10^5 cells/well in a 6-well plate in αMEM medium containing 10% FBS and cultured for 24 hours. They were then treated with 0μg/mL (control group) and 200μg/mL PL-CQDs (CQDs group) for 24 hours. Total RNA was extracted with Trizol reagent, and 1μg of each sample was used for RNA sample preparation. Sequencing libraries were generated using the NEBNext® Ultra™ RNA Library Prep Kit for Illumina® (NEB, California, USA) according to the manufacturer's protocol, with index codes added to the attribute sequence of each sample. The library quality was assessed by the Agilent Bioanalyzer 2100 system. Clustering of index-encoded samples was performed using TruSeq PE Cluster Kit v3-cBot-HS (Illumia) on cBot Cluster Generation System, following the manufacturer's instructions. After cluster generation, the library preparations were sequenced on the Illumina platform and paired-end reads were generated. The raw reads were further processed using the bioinformatics pipeline tool BMKCloud online platform (www.biocloud.net). Differential expression analysis was performed using DESeq2. The resulting P-values were adjusted using the Benjamini and Hochbergs method to control the false discovery rate (FDR). Genes with adjusted P-values < 0.05 found by DESeq2 were designated as differentially expressed. Gene Ontology (GO) enrichment analysis of differentially expressed genes (DEGs) was determined based on the Wallenius noncentral hypergeometric distribution using GOseq R package.[26] KOBAS software was used to test the statistical enrichment of differentially expressed genes in Kyoto Encyclopedia of Genes and Genomic (KEGG) pathways.[27]

Vivo Therapeutic Efficacy of PL-CQDs@CS in Osteomyelitis

Thirty Sprague-Dawley rats were used to establish the osteomyelitis model. After isoflurane anesthesia, each animal was drilled with a 2mm-diameter drill for 4mm depth at the lateral condyle of the right distal femur, and 3 μL of sodium morrhuate (Xinyi Jinzhu Pharmaceutical Co., Ltd., Shanghai, China) was injected into the hole. After 5 minutes, 10 μL of USA300 bacterial solution (3×10^6 CFU/mL) was injected and the hole sealed with bone wax to induce osteomyelitis.

One week later, the skin was cut along the original incision for debridement. Specifically, a 3mm-diameter drill was used to create a 5 mm deep hole at the original femoral condyle to remove infected and necrotic bone tissue. After flushing with iodine and saline, the pre-made cylindrical with different material proportions (Table 1) was filled into the femoral condyle defect, and the empty defect was used as a control. At 4 and 8 weeks after treatment, three rats in each group were euthanized, and the right femurs were harvested for micro-CT imaging and histological staining analysis.

Imaging Analyses

High-resolution scanning was performed using a micro-CT (SkyScan 1174, Kontich, Belgium). The micro-CT images were then three-dimensionally (3D) reconstructed using CT-Vox software (version 2.0.0, Kontich, Belgium) and analyzed with CTAn software (version 1.16.4.1, Bruker, Belgium). The defect site was selected as the region of interest (ROI) and analyzed to calculate the new bone volume (BV) and the percentage of BV relative to tissue volume (BV/TV).

Histological Analysis

After imaging analysis, femoral specimens were processed for histological analysis. The specimens were fixed in 4% neutral buffered formalin for 24 h, decalcified in 12.5% EDTA (Biyuntian Biotechnology Co., Ltd., Shanghai, China), dehydrated in graded ethanol and embedded in paraffin. The specimens were cut into 5 μm thick sections using a microtome (RM2255, Leica Microsystems, Germany). The sections were stained using Masson's trichrome for histological evaluation. Additionally, the expression of CD31 (antibody: ab236639, Abcam, USA) and DMP1 (antibody: AF4386, R&D Systems, Inc. a Bio-Techne Brand, Minneapolis, MN, USA) in sections from the material implantation area was detected by immunohistochemistry.

Statistical Analysis

All experiments were performed in triplicate, and the data presented are the averages from three independent experiments. Data are presented as mean ± standard deviation (SD). Comparisons between samples were performed using the Student's *t*-test. For multiple group comparisons, one-way analysis of variance (ANOVA) was used, with post-hoc corrections applied using the Bonferroni method. $P < 0.05$ was considered statistically significant.

Results

Characterization of PL-CQDs

The PL-CQDs synthesized by dry heat-intermittent ultrasound method (Figure 1A) exhibited excellent dispersibility in water, with no obvious aggregation observed by TEM and the HRTEM shows that the lattice spacing is about 0.20 nm (Figure 1B). The PL-CQDs are uniformly spherical in shape with a particle size of (2.00±0.68) nm (Figure 1C). When PL-CQDs were doped into CS, TEM and HRTEM observed that the density of PL-CQDs in the composite material increased with the increase of PL-CQDs doping concentration, but the original lattice was still retained (Figure S1). The PL-CQDs solution exhibited obvious photoluminescence under ultraviolet light excitation (Figure 1D) and the ultraviolet absorption spectrum showed that PL-CQDs had two distinct absorption peaks at 210nm and 300nm (Figure 1E). Additionally, the emission spectrum exhibited a significant red shift as the excitation wavelength increased from 320 nm to 480 nm(Figure 1F). Zeta potential measurements indicated that PL-CQDs carried a positive charge of 44.13 ± 0.64 mV (Figure 1G). The FTIR analysis confirmed that PL-CQDs had a different chemical structure compared to the precursor molecule ε-poly (L-lysine), indicating the chemical conversion of ε-poly (L-lysine) to PL-CQDs. The FTIR results also showed that the peaks at 3424 cm^{-1} and 2931 cm^{-1} represent the stretching vibrations of N-H in the amide group and C-H, respectively. The two peaks near 1600 cm^{-1} (1653 cm^{-1} and 1450 cm^{-1}) correspond to the stretching vibration of C=O and the bending vibration of N-H in the amide group, respectively (Figure 1H). The findings suggest that PL-CQDs are rich in amino and hydroxyl groups, contributing to their good water solubility. Degradation test demonstrated that the composite materials with different concentrations of PL-CQDs degrade gradually over time in PBS at 37°C, with no significant difference observed among the various groups (Figure 1I).

 https://doi.org/10.2147/IJN.S521727

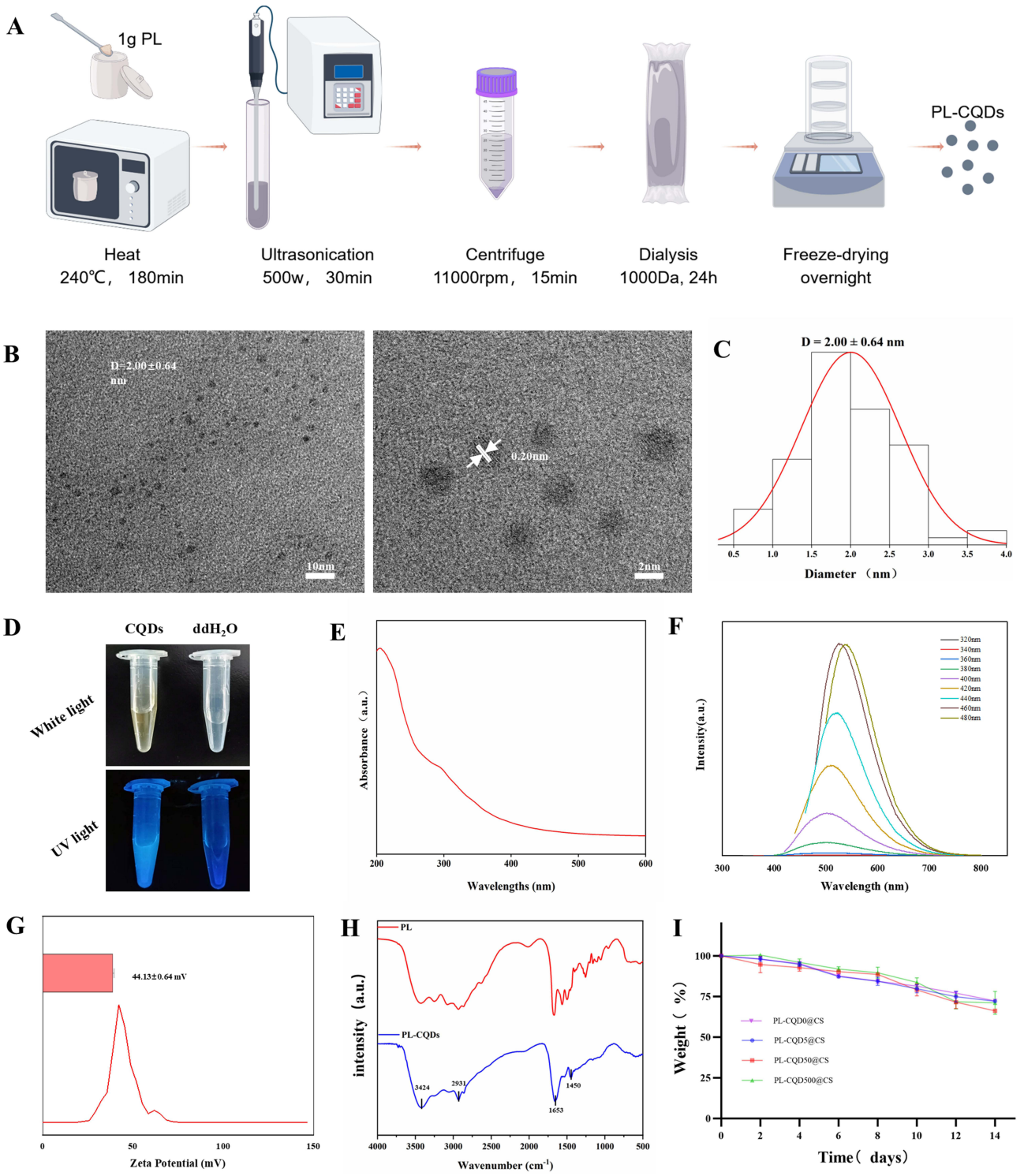

Figure 1 Synthesis and characterization of PL-CQDs. (**A**) Schematic diagram of the synthesis of PL-CQDs by dry heat-intermittent ultrasound method (created online via http://www.figdraw.com), (**B**) TEM image (scale bar: 10 nm) and HRTEM image (scale bar: 2 nm) of PL-CQDs, (**C**) Size distribution of PL-CQDs measured by TEM, (**D**) Luminescence phenomenon of PL-CQDs solution and deionized water under white light (top) and ultraviolet light (bottom), (**E**) UV excitation spectrum of PL-CQDs, (**F**) Photoluminescence spectrum of PL-CQDs, (**G**) Zeta potential of PL-CQDs, (**H**) FTIR spectrum of PL-CQDs and ε-poly (L-lysine), (**I**) Degradation curve of the composite material.

PL-CQDs Have No Significant Cytotoxicity

The CCK-8 assay indicated that PL-CQDs exhibited favorable biocompatibility in vitro. Concentrations of 200, 400, and 800 μg/mL of PL-CQDs did not demonstrate significant cytotoxic effects on MC3T3-E1 cells and were observed to

enhance cell proliferation (P<0.05, compared to the control group). In contrast, at a higher concentration of 1600 μg/mL, PL-CQDs significantly inhibited cell proliferation (Figure 2A). The live/dead assay corroborated these results, showing consistent findings (Figure 2B).

PL-CQDs Have in vitro Antibacterial Effects and Promotes the Differentiation and Migration of Osteoblasts

The spread plate method (SPM) was used to evaluate the antibacterial activity of PL-CQDs against MRSA and *E. coli*. The results indicated that the bactericidal effect of PL-CQDs increased with their concentration within safe limits for cells (Figure 3A). At a concentration of 400μg/mL, both MRSA and *E. coli* in the test solution were nearly eradicated (Figure 3B and C). After treating MRSA and *E. coli* with 800μg/mL of PL-CQDs for 1 hour, SEM revealed that the surfaces of both MRSA and *E. coli* in the experimental group were covered with numerous small particles. We speculate that this may be due to the adsorption of PL-CQDs caused by charge interactions. Additionally, phenomena such as bacterial death and shrinkage were observed in the experimental group, whereas these were absent in the control group (Figure 3D).

To investigate the impact of PL-CQDs on the biological function of MC3T3-E1 cells, we performed in vitro osteogenic differentiation assay and scratch assay. Before the addition of CS, the level of calcified nodule deposition in the PL-CQDs group after three weeks of osteogenic induction was significantly higher compared to the control group (P<0.05). Upon the supplementation of CS, the osteogenic differentiation capacity improved in all groups. The PL-CQDs group supplemented with CS did not show a significant difference compared to the control group with CS (P=0.43), but demonstrated a significantly enhanced osteogenic differentiation ability compared to the control group without CS (P<0.01) (Figure 4A and B). The results of scratch assay indicated that the wound healing rate in the group treated with 200 μg/mL PL-CQDs was significantly higher than that of the control group (82.89% ± 1.742% vs 52.30% ± 2.42%; P<0.001). However, when the concentration was increased to 400 μg/mL, the wound closure rate, although still greater than the control group (61.11% ± 2.20% vs 52.30% ± 2.42%; P=0.006), was lower than that observed in the 200 μg/mL group (Figure 4C and D).

PL-CQDs promote MC3T3-E1 to participate in biological processes, including positive regulation of chondrocyte proliferation, collagen fiber organization, and regulation of fibroblast proliferation

To further investigate the mechanisms underlying the biological effects of PL-CQDs on MC3T3-E1 cells, we conducted transcriptome sequencing following stimulation of MC3T3-E1 cells with 0 μg/mL (control group) and 200 μg/mL PL-CQDs

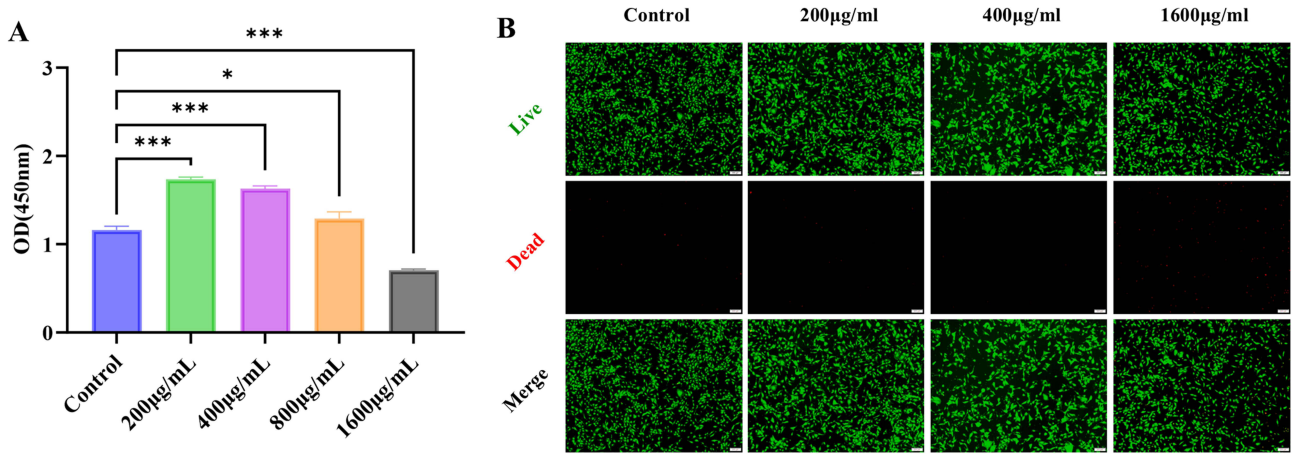

Figure 2 Cytotoxicity experiment of PL-CQDs. (**A**) CCK-8 assay results, (**B**) Live/dead assay results. (n = 3; ns represents P > 0.05, * represents P < 0.05, *** represents P < 0.001).

https://doi.org/10.2147/IJN.S521727

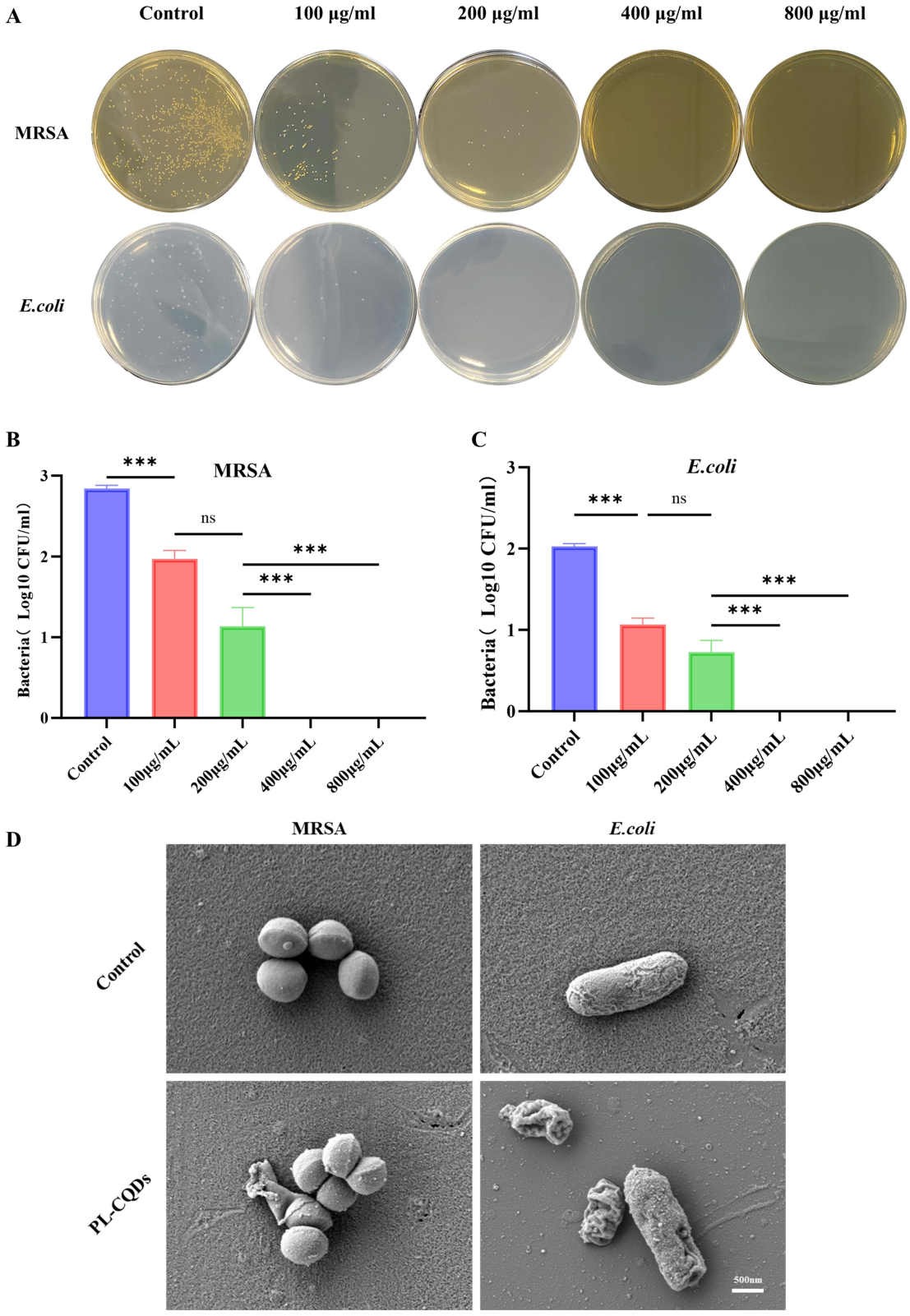

Figure 3 Antibacterial efficacy of PL-CQDs. (**A**) a) Spread plate of MRSA and *E. Coli* treated with different concentrations of PL-CQDs, (**B, C**) Antibacterial efficiency against MRSA and *E. Coli* with different concentrations of PL-CQDs (n = 3; ns represents P > 0.05, *** represents P < 0.001), (**D**) SEM of images of different treatment groups (scale bar: 500nm).

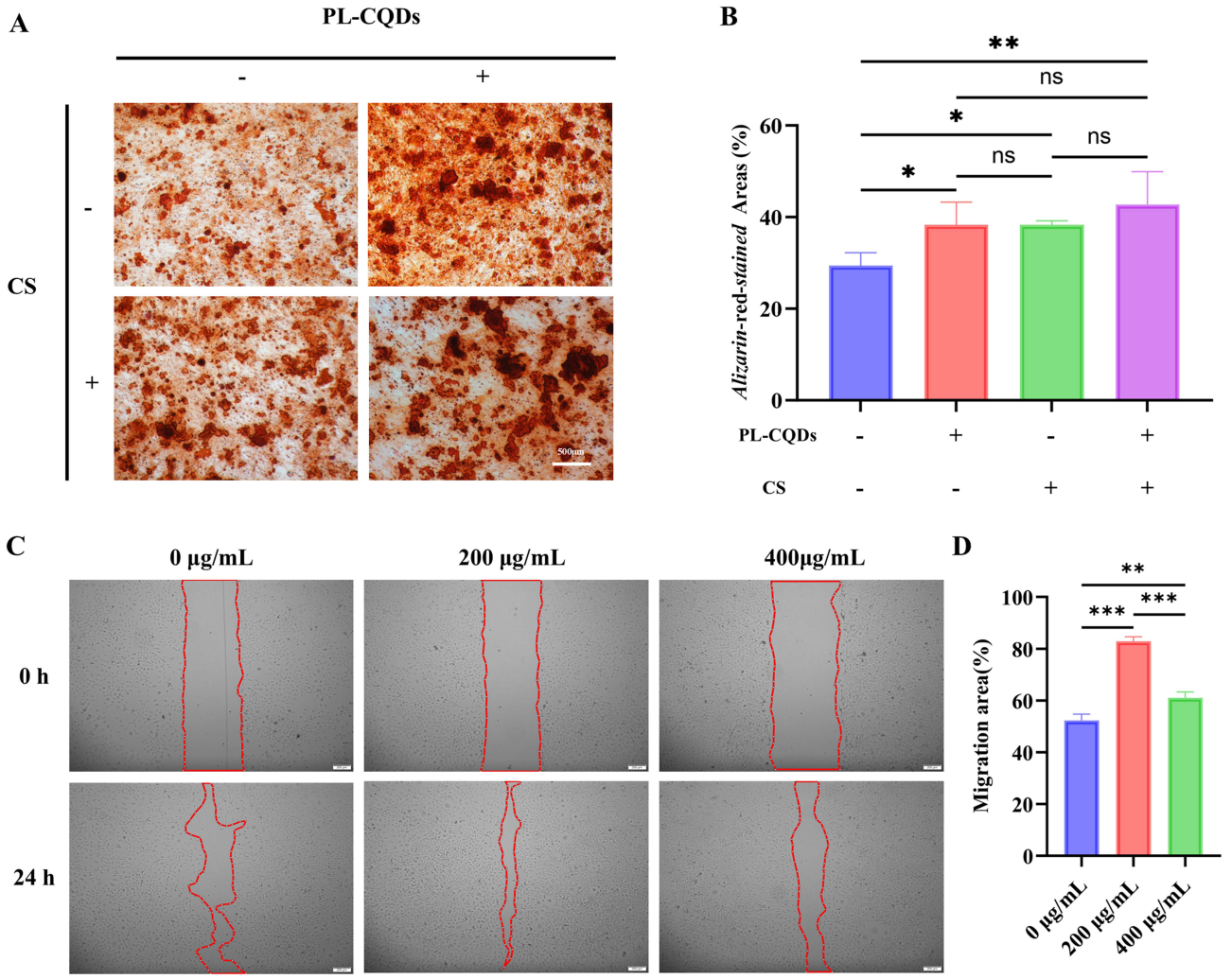

Figure 4 Biological effects of PL-CQDs on MC3T3-E1 cells. (**A**) Alizarin red staining (scale bar: 500μm), (**B**) Quantification of alizarin red staining, (**C**) Representative images of wound healing scratch assay (scale bar: 200μm), (**D**) Migration rate of cell migration by wound healing assay. (n = 3; ns represents P > 0.05,* represents P < 0.05, ** represents P < 0.01,*** represents P < 0.001).

(PL-CQDs group). Using a FoldChange threshold of ≥1.5 and a P-value of <0.05 as the screening criteria, we identified a total of 233 DEGs, with 131 genes being upregulated and 102 downregulated (Figure 5A). KEGG enrichment analysis of these DEGs revealed that PL-CQDs significantly alter the ECM-receptor for interaction signaling pathway (Figure 5B), which is potentially linked to extracellular matrix secretion and mineralization in MC3T3-E1 cells. GO enrichment analysis further demonstrated that exposure to 200 μg/mL PL-CQDs enhances mRNA expression associated with biological processes such as positive regulation of chondrocyte proliferation, collagen fiber organization, and regulation of fibroblast proliferation (Figure 5C). Additionally, we analyzed DEGs involved in regulation of bone mineralization, positive regulation of cell migration, ossification, focal adhesion, extracellular matrix organization, ECM-receptor interaction, collagen fiber organization, and cell adhesion. The results indicated that 76% of these genes were upregulated, with the majority associated with extracellular matrix deposition and mineralization. These included genes such as *Itgb7, Col2a1, Grem1, Dmp1, Ctsk, Scube2, Vwf, Tnxb, Tnr*, and *Lef1*(Figure 5D). Notably, genes like Lef1 also contribute to cell migration.

PL-CQDs@CS Promote Bone Defect Repair in Osteomyelitis

To evaluate the therapeutic efficacy of PL-CQDs@CS in osteomyelitis, an osteomyelitis model was successfully established (Figure 6A). Following model induction, rats exhibited increased body temperature, which returned to normal after one week, and local pus exudation was also observed (Figure S2). However, after the second-stage surgery

https://doi.org/10.2147/IJN.S521727

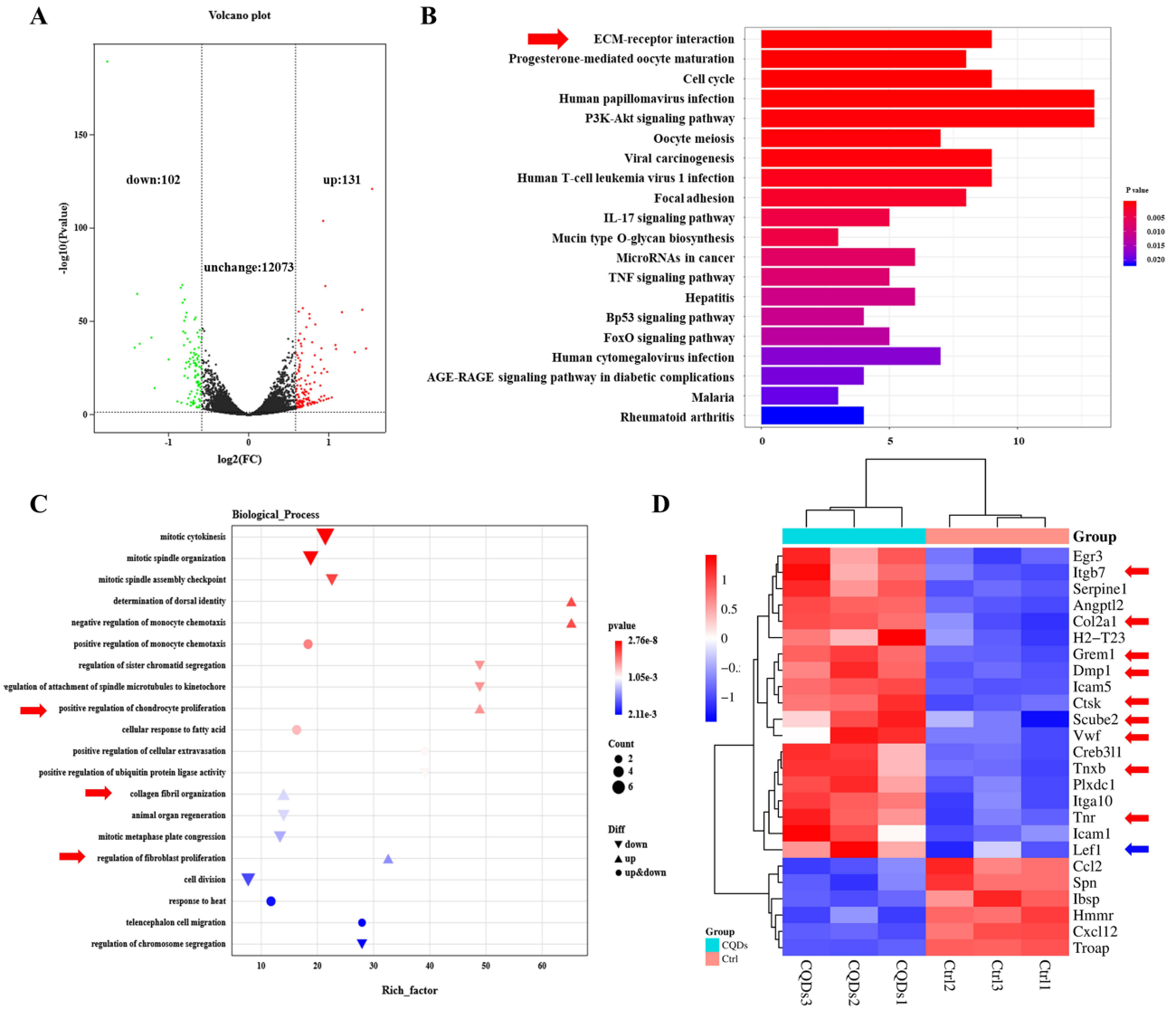

Figure 5 Transcriptome sequencing results. (**A**) Volcano plot of differential gene expression analysis, (**B**) KEGG pathway analysis of DEGs, (**C**) GO enrichment analysis of DEGs, (**D**) Heat map of DEGs related to regulation of bone mineralization, positive regulation of cell migration, ossification, focal adhesion, extracellular matrix organization, ECM-receptor interaction, collagen fiber organization, and cell adhesion.

involving debridement and material implantation, no obvious signs of infection, such as redness, increased body temperature, and pus exudation, were observed in any of the groups. Micro-CT reconstruction imaging revealed that at 4 weeks, only a minimal amount of new bone formation was observed in the control group. In contrast, the groups treated with different concentrations of PL-CQDs exhibited varying degrees of increased bone formation, with the PL-CQD50@CS group demonstrating the most significant increase. This trend persisted at 8 weeks, mirroring the observations at 4 weeks (Figure 6B). Subsequently, bone morphometric parameters of the ROIs were calculated using specialized analytical software to quantitatively assess new bone regeneration. The results indicated that BV and BV/TV exhibited similar trends. Specifically, the BV and BV/TV values of the PL-CQD50@CS group were consistently higher than those of the control group and other PL-CQDs concentration groups at all examined time points (Figure 6C and D). These findings suggested that the incorporation of PL-CQDs is beneficial for the repair of bone defects in osteomyelitis, but excessive concentrations may have inhibitory effects.

Masson staining revealed histological alterations at the bone defect site. The results indicated that bone infection in the control group was not effectively controlled, leading to further exacerbation of bone damage. In contrast, bone infection in the groups implanted with each material was effectively managed, as evidenced by a reduced size of the bone defect. Additionally,

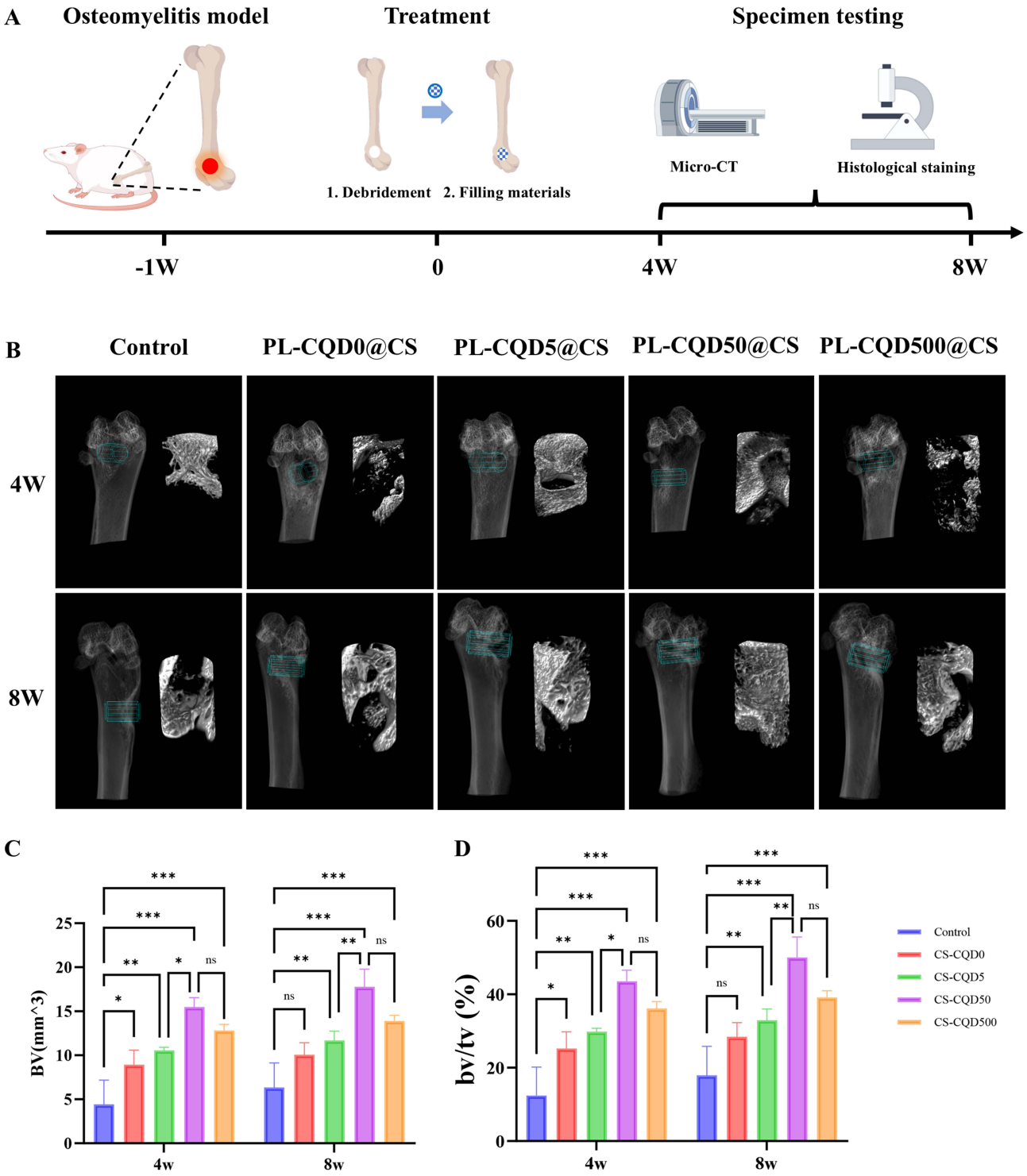

Figure 6 Therapeutic Efficacy of PL-CQDs@CS in an Osteomyelitis Model. (**A**) Schematic diagram of osteomyelitis modeling and treatment protocol (created online via www.figdraw.com), (**B**) Micro-CT images of femurs from each experimental group at 4 and 8 weeks post-surgery, (**C** and **D**) Quantitative analysis of bone morphometric parameters within the ROIs. (n = 3; ns represents P > 0.05,* represents P < 0.05, ** represents P < 0.01,*** represents P < 0.001).

Masson staining of collagen fibers (stained blue) demonstrated that the incorporation of PL-CQDs increased collagen fiber deposition, with the PL-CQD50@CS group exhibiting the most pronounced effect (Figure 7A). Immunohistochemical analysis showed that PL-CQDs significantly enhanced the expression of CD31-positive cells at the infectious bone defect site at 4 weeks, indicating their ability to promote vascularization at the defect site (Figure 7A and B). At 8 weeks, DMP1

https://doi.org/10.2147/IJN.S521727

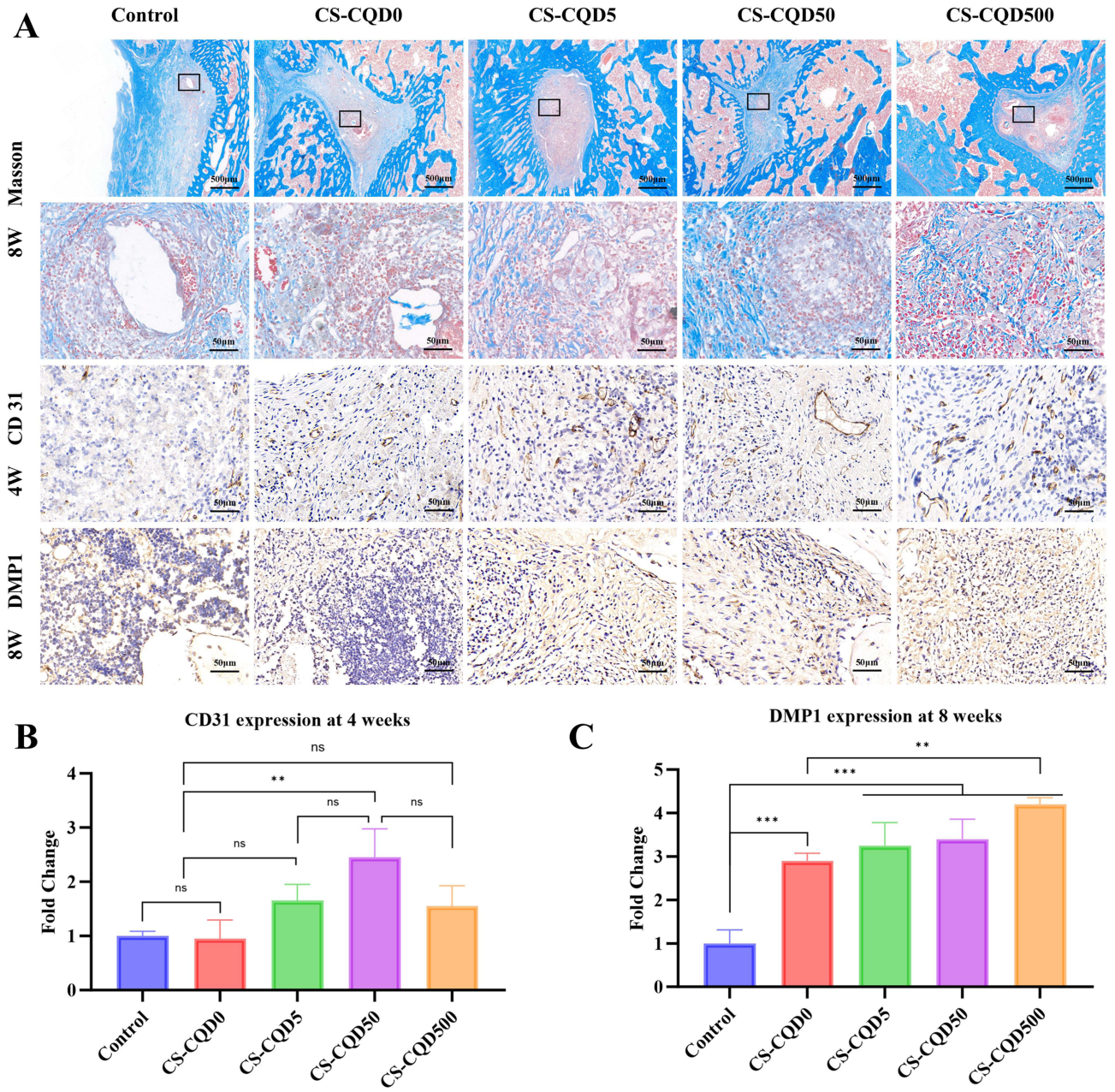

Figure 7 Histological analysis of bone tissue in rats from each group at 4 and 8 weeks post-surgery.(**A**) Masson's trichrome staining and immunohistochemical staining, (**B**) CD31 expression levels in each treatment group at 4 weeks, (**C**) DMP1 expression levels in each treatment group at 8 weeks. (n = 3; ns represents P > 0.05,** represents P < 0.01,*** represents P < 0.001).

staining in the extracellular matrix of the PL-CQDs group was elevated compared to the control group, suggesting that PL-CQDs may facilitate extracellular matrix deposition and mineralization via DMP1 (Figure 7A and C). Histological examination of major organs, including the heart, liver, spleen, lung, and kidney, using hematoxylin and eosin (H&E) staining revealed intact tissue architecture with no evident infiltration or destruction by inflammatory cells. This finding indicates that PL-CQDs exhibit favorable biocompatibility (Figure S3).

Discussion

The management of osteomyelitis remains a formidable clinical challenge. The advent of antibiotics initially ushered in a brief era of significant advancements in treating this condition. However, the emergence of antibiotic-resistant strains

has once again complicated treatment strategies. Current clinical guidelines advocate for thorough surgical debridement combined with systemic antibiotic therapy.[28] Despite these efforts, the outcomes have been suboptimal, with data indicating persistently high recurrence rates.[1] The escalating crisis of antibiotic resistance has compelled researchers to explore novel antibacterial strategies.[29] Moreover, the repair of infectious bone defects poses additional difficulties. Research has shown that the surface properties of *S. aureus* and its secreted molecules can directly or indirectly inhibit osteoblasts, activate osteoclasts, induce cell death, diminish bone formation, and promote bone resorption.[30,31] In recent years, advancements in biomaterial science have introduced new hope for the treatment of osteomyelitis. A multitude of novel materials with both antibacterial efficacy and osteogenic properties have been developed. In vitro and in vivo studies in the animal models have confirmed their therapeutic potential.[32–34] However, the complex manufacturing processes associated with many of these materials preclude large-scale production. Consequently, only a limited number of such products have transitioned into clinical use.

In our study, the composite material employed for the treatment of the osteomyelitis consists of two distinct components. One component is carbon quantum dots (PL-CQDs), which exhibit antibacterial efficacy, while the other is a commercially available artificial bone product with osteogenic properties (OSTEOSET®). The PL-CQDs are synthesized via a dry heat-intermittent ultrasound method, which is characterized by its simplicity and stability. The raw material utilized for the synthesis is ε-poly (L-lysine), a natural biological metabolite that is widely available and possesses favorable bactericidal and thermal stability properties.[35] The synthesized PL-CQDs have a particle size of less than 10 nm and can be uniformly dispersed in both deionized water and calcium sulfate bone substitutes without significant aggregation. These quantum dots retain the lattice stripes of the original graphene structure, which is advantageous for their carbon-based properties. The stable and slow release of the quantum dots at the lesion site ensures prolonged retention of PL-CQDs, thereby enhancing the therapeutic effect.[36] FTIR analysis revealed that PL-CQDs exhibit the same amino absorption peak as their raw material, which is closely associated with their superior solubility. Moreover, PL-CQDs possess photoluminescent properties under ultraviolet light excitation and this characteristic have been utilized as a tracer for bioimaging in several studies.[37] However, the most remarkable aspect of PL-CQDs is their biological properties. Literature reports indicate that carbon quantum dots synthesized by bottom-up methods using ε-poly (L-lysine) as a precursor exhibit excellent biocompatibility and display high antibacterial activity against *Enterococcus faecalis*. Similarly, PL-CQDs synthesized by analogous methods have demonstrated potent antibacterial activity against MRSA and *E.coli*[25.] Although we did not further investigate the antibacterial mode and mechanism of PL-CQDs, previous studies suggest that their ultra-small size and high positive charge may play a crucial role.[25,38] Positively charged carbon quantum dots have been reported to electrostatically adsorb to bacterial surfaces[39] and easily penetrate biofilms,[10,25] thereby exerting a sterilizing effect.

In vitro experiments have demonstrated that PL-CQDs favorably influence cell proliferation and migration and partially promote osteogenic differentiation. Two studies have shown that positively charged carbon quantum dots (pCQDs) do not affect the osteogenic differentiation of mesenchymal stem cells, whereas negatively charged CQDs (nCQDs) can significantly enhance this process. This enhancement may be attributed to the interaction between nCQDs and positively charged bone morphogenetic proteins (BMPs), which can induce increased BMPs expression, promote Smad1/5 phosphorylation, and subsequently upregulate the expression of osteogenesis-related genes and proteins.[18,40] Nevertheless, our sequencing results indicate that despite being positively charged, PL-CQDs exert a promoting effect on several biological processes, including the positive regulation of chondrocyte proliferation, collagen fiber organization, and fibroblast proliferation. These processes are closely associated with bone defect repair. Specifically, we found that PL-CQDs can upregulate the expression of genes such as *Dmp1, Col2a1*, and *Grem1*. *Dmp1* is a key gene involved in these biological processes, encoding dentin matrix protein 1 (DMP1), a non-collagenous component of the extracellular matrix that regulates osteoblast differentiation and maturation and participates in the bone mineralization process.[41,42] After 8 weeks of PL-CQDs@CS treatment, immunohistochemical analysis of bone tissue confirmed an increase in DMP1 expression. *Col2a1* encodes collagen alpha-1(II) chain, which is essential for normal bone and cartilage development and endochondral ossification.[43] Masson staining revealed enhanced collagen deposition following PL-CQDs@CS treatment. Additionally, genes involved in cell adhesion, such as *Vwf, Icam5*, and *Cxcl12*, are upregulated in response to PL-CQDs stimulation. The cytokines or proteins encoded by these genes may play crucial roles in bone defect repair. Therefore, it is hypothesized that PL-CQDs may promote bone repair by enhancing the synthesis and/or secretion of these cytokines and proteins. CD31, a marker of H-type endothelial cells, is involved in the

vascularization-osteogenesis coupling process and is vital for bone formation and maintenance of bone homeostasis.[44] Immunohistochemical analysis of rat bone tissue at 4 weeks showed that treatment with PL-CQDs increased CD31 expression, suggesting another potential mechanism by which PL-CQDs promote bone defect repair. However, these mechanisms need to be further verified through polymerase chain reaction (PCR) and Western Blot (WB) experiments. This represents a limitation of our current study.

The other component of the composite material is derived from a commercial CS bone substitute. In this study, it served as a carrier for PL-CQDs. Upon implantation, the CS rapidly degrades, releasing the incorporated PL-CQDs and creating a calcium-rich environment that facilitates biological reactions and initiates the bone regeneration process.[45] In the preparation of the composite material, we employed a straightforward physical incorporation method, which may appear less innovative. However, compared to more complex strategies, such as depositing multidrug-resistant (MDR) bacteria-killing pCQDs onto WS_2 nanosheets, and subsequently combining them with nCQDs that enhance osteogenic differentiation to form a three-dimensional hydrogel, the primary advantage of our approach is its simplicity and ease of implementation.[18] This method closely aligns with existing osteomyelitis treatment products that have already transitioned into clinical use[46,47.]

Conclusion

In summary, PL-CQDs prepared via a simple method exhibit robust antibacterial effects, which can be attributed to their ultra-small size and high positive charge. Both in vitro cellular experiments and in vivo animal studies demonstrate that PL-CQDs can effectively promote osteogenic differentiation and repair the bone defects in osteomyelitis, while maintaining excellent biocompatibility. Therefore, PL-CQDs offer a novel therapeutic strategy for the treatment of osteomyelitis and hold potential for practical clinical application.

Acknowledgments

This work was funded by Chongqing Medical Scientific Research Project (2024QNXM035).

Disclosure

The authors report no conflicts of interest in this work.

References

1. Veis DJ, Cassat JE. Infectious osteomyelitis: marrying bone biology and microbiology to shed new light on a persistent clinical challenge. *J Bone Miner Res*. 2021;36(4):636–643. doi:10.1002/jbmr.4279
2. Jiang N, Zhao X, Qin C, et al. Association of vitamin d receptor gene TaqI, BsmI, FokI and ApaI polymorphisms and susceptibility to extremity chronic osteomyelitis in Chinese population. *Injury*. 2016;47(8):1655–1660. doi:10.1016/j.injury.2016.06.005
3. Ren Y, Liu L, Sun D, et al. Epidemiological updates of post-traumatic related limb osteomyelitis in China: a 10 years multicentre cohort study. *Int J Surg*. 2023;109(9):2721–2731. doi:10.1097/JS9.0000000000000502
4. Masters EA, Ricciardi BF, Bentley KLDM, Moriarty TF, Schwarz EM, Muthukrishnan G. Skeletal infections: microbial pathogenesis, immunity and clinical management. *Nat Rev Microbiol*. 2022;20(7):385–400. doi:10.1038/s41579-022-00686-0
5. Li H, Rombach I, Zambellas R, et al. Oral versus intravenous antibiotics for bone and joint infection. *N Engl J Med*. 2019;380(5):425–436. doi:10.1056/NEJMoa1710926
6. Anagnostakos K, Wilmes P, Schmitt E, Kelm J. Elution of gentamicin and vancomycin from polymethylmethacrylate beads and Hip spacers in vivo. *Acta Orthop*. 2009;80(2):193–197. doi:10.3109/17453670902884700
7. Gimza BD, Cassat JE. Mechanisms of antibiotic failure during staphylococcus aureus osteomyelitis. *Front Immunol*. 2021;12:638085. doi:10.3389/fimmu.2021.638085
8. Xu Z, Xia Y, Zhou P, et al. Silicon incorporation into hydroxyapatite nanocarrier counteracts the side effects of vancomycin for efficient chronic osteomyelitis treatment. *Chem Eng J*. 2021;406(13):126821. doi:10.1016/j.cej.2020.126821
9. Li J, Yang S, Liu Z, et al. Imaging cellular aerobic glycolysis using carbon dots for early warning of tumorigenesis. *Adv Mater*. 2021;33(1):e2005096. doi:10.1002/adma.202005096
10. Wang H, Song Z, Gu J, Li S, Wu Y, Han H. Nitrogen-doped carbon quantum dots for preventing biofilm formation and eradicating drug-resistant bacteria infection. *ACS Biomater Sci Eng*. 2019;5(9):4739–4749. doi:10.1021/acsbiomaterials.9b00583
11. Anand A, Unnikrishnan B, Wei S, Chou CP, Zhang L, Huang C. Graphene oxide and carbon dots as broad-spectrum antimicrobial agents - a minireview. *Nanoscale Horiz*. 2019;4(1):117–137. doi:10.1039/c8nh00174j
12. Tang C, Liu C, Han Y, et al. Nontoxic carbon quantum dots/g-c(3) n(4) for efficient photocatalytic inactivation of staphylococcus aureus under visible light. *Adv Healthc Mater*. 2019;8(10):e1801534. doi:10.1002/adhm.201801534
13. Li H, Huang J, Song Y, et al. Degradable carbon dots with broad-spectrum antibacterial activity. *ACS Appl Mater Interfaces*. 2018;10(32):26936–26946. doi:10.1021/acsami.8b08832

14. Tang T, Liu Y, Wang P, et al. Carbon quantum dots as a nitric oxide donor can promote wound healing of deep partial-thickness burns in rats. *Eur J Pharm Sci*. 2023;183:106394. doi:10.1016/j.ejps.2023.106394
15. Mei L, Gao X, Shi Y, et al. Augmented graphene quantum dot-light irradiation therapy for bacteria-infected wounds. *ACS Appl Mater Interfaces*. 2020;12(36):40153–40162. doi:10.1021/acsami.0c13237
16. Liang M, Wang Y, Ma K, et al. Engineering inorganic nanoflares with elaborate enzymatic specificity and efficiency for versatile biofilm eradication. *Small*. 2020;16(41):e2002348. doi:10.1002/smll.202002348
17. Guo Z, Wang Z, Liu Y, et al. Carbon Dots from Lycium barbarum Attenuate Radiation-Induced Bone Injury by Inhibiting Senescence via METTL3/Clip3 in an m(6)A-Dependent Manner. *ACS Appl Mater Interfaces*. 2023;15(17):20726–20741. doi:10.1021/acsami.3c01322.19
18. Geng B, Li P, Fang F, et al. Antibacterial and osteogenic carbon quantum dots for regeneration of bone defects infected with multidrug-resistant bacteria. *Carbon*. 2021;184:375–385. doi:10.1016/j.carbon.2021.08.040
19. Lew DP, Waldvogel FA. Osteomyelitis. *Lancet*. 2004;364(9431):369–379. doi:10.1016/S0140-6736(04)16727-5
20. Vallon F, Meier C, Gautier E, Wahl P. The incidence of severe hypercalcaemia-induced mental status changes in patients treated with antibiotic-loaded calcium sulphate depot for orthopaedic infections. *J Clin Med*. 2022;11(16):9. doi:10.3390/jcm11164900
21. Gupta H, Pandey A, Agarwal R, et al. Application of calcium sulfate as graft material in implantology and maxillofacial procedures: a review of literature. *Natl J Maxillofac Surg*. 2024;15(2):183–187. doi:10.4103/njms.njms_33_22
22. Cho BC, Park JW, Baik BS, Kim IS. Clinical application of injectable calcium sulfate on early bony consolidation in distraction osteogenesis for the treatment of craniofacial microsomia. *J Craniofac Surg*. 2002;13(3):465–475,475–477. doi:10.1097/00001665-200205000-00019
23. Barrere F, van Blitterswijk CA, de Groot K. Bone regeneration: molecular and cellular interactions with calcium phosphate ceramics. *Int J Nanomed*. 2006;1(3):317–332.
24. Ferguson JY, Dudareva M, Riley ND, Stubbs D, Atkins BL, Mcnally MA. The use of a biodegradable antibiotic-loaded calcium sulphate carrier containing tobramycin for the treatment of chronic osteomyelitis: a series of 195 cases. *Bone Joint J*. 2014;96-B(6):829–836. doi:10.1302/0301-620X.96B6.32756
25. Xu Y, Hao Y, Arif M, et al. Poly(lysine)-derived carbon quantum dots conquer enterococcus faecalis biofilm-induced persistent endodontic infections. *Int J Nanomed*. 2024;19:5879–5893. doi:10.2147/IJN.S453385
26. Young MD, Wakefield MJ, Smyth GK, Oshlack A. Gene ontology analysis for RNA-seq: accounting for selection bias. *Genome Biol*. 2010;11(2):R14. doi:10.1186/gb-2010-11-2-r14
27. Mao X, Cai T, Olyarchuk JG, Wei L. Automated genome annotation and pathway identification using the KEGG orthology (KO) as a controlled vocabulary. *Bioinformatics*. 2005;21(19):3787–3793. doi:10.1093/bioinformatics/bti430
28. Govaert GAM, Kuehl R, Atkins BL, et al. Diagnosing fracture-related infection: current concepts and recommendations. *J Orthop Trauma*. 2020;34(1):8–17. doi:10.1097/BOT.0000000000001614
29. Ren J, Qiao Y, Jin L, et al. A smart bacteria-capture-killing vector for effectively treating osteomyelitis through synergy under microwave therapy. *Small*. 2024;20(15):e2307406. doi:10.1002/smll.202307406
30. Bertelli AM, Delpino MV, Lattar S, et al. Staphylococcus aureus protein a enhances osteoclastogenesis via TNFR1 and EGFR signaling. *Biochim Biophys Acta*. 2016;1862(10):1975–1983. doi:10.1016/j.bbadis.2016.07.016
31. Ren L, Wang H, He X, Song M, Chen X, Xu Y. Staphylococcus aureus protein a induces osteoclastogenesis via the NF-kappab signaling pathway. *Mol Med Rep*. 2017;16(5):6020–6028. doi:10.3892/mmr.2017.7316
32. Fang B, Qiu P, Xia C, et al. Extracellular matrix scaffold crosslinked with vancomycin for multifunctional antibacterial bone infection therapy. *Biomaterials*. 2021;268:120603. doi:10.1016/j.biomaterials.2020.120603
33. Ma L, Cheng Y, Feng X, et al. A janus-ROS healing system promoting infectious bone regeneration via sono-epigenetic modulation. *Adv Mater*. 2024;36(2):e2307846. doi:10.1002/adma.202307846
34. Fu J, Li Y, Zhang Y, et al. An engineered pseudo-macrophage for rapid treatment of bacteria-infected osteomyelitis via microwave-excited anti-infection and immunoregulation. *Adv Mater*. 2021;33(41):e2102926. doi:10.1002/adma.202102926
35. Wang M, Rong C. Poly(epsilon-l-lysine) and poly(l-diaminopropionic acid) co-produced from spent mushroom substrate fermentation: potential use as food preservatives. *Bioengineered*. 2022;13(3):5892–5902. doi:10.1080/21655979.2022.2040876
36. Li X, Huang R, Tang F, et al. Red-emissive guanylated polyene-functionalized carbon dots arm oral epithelia against invasive fungal infections. *ACS Appl Mater Interfaces*. 2019;11(50):46591–46603. doi:10.1021/acsami.9b18003
37. Ai L, Yang Y, Wang B, et al. Insights into photoluminescence mechanisms of carbon dots: advances and perspectives. *Sci Bull*. 2021;66(8):839–856. doi:10.1016/j.scib.2020.12.015
38. Mandal H, Katiyar SS, Swami R, et al. Epsilon-poly-l-lysine/plasmid DNA nanoplexes for efficient gene delivery in vivo. *Int J Pharm*. 2018;542(1–2):142–152. doi:10.1016/j.ijpharm.2018.03.021
39. Li P, Sun L, Xue S, et al. Recent advances of carbon dots as new antimicrobial agents. *SmartMat*. 2022;3(2):226–248. doi:10.1002/smm2.1131
40. Geng B, Fang F, Li P, et al. Surface charge-dependent osteogenic behaviors of edge-functionalized graphene quantum dots. *Chem Eng J*. 2021;417:128125. doi:10.1016/j.cej.2020.128125
41. Jin N, Jin N, Wang Z, et al. Osteopromotive carbon dots promote bone regeneration through the PERK-eIF2α-ATF4 pathway. *biomaterials Science*. 2020;8(10):2840–2852. doi:10.1039/d0bm00424c
42. Wu L, Wu Y, Jingjin L, et al. Calcium and phosphorus co-doped carbon dots enhance osteogenic differentiation for calvarial defect repair in situ. *Biomed Mater*. 2022;17(5):055007. doi:10.1088/1748-605X/ac812f
43. Rolvien T, Yorgan TA, Kornak U, et al. Skeletal deterioration in COL2a1-related spondyloepiphyseal dysplasia occurs prior to osteoarthritis. *Osteoarthritis Cartilage*. 2020;28(3):334–343. doi:10.1016/j.joca.2019.12.011
44. He W, Yang M, Jiang Y, et al. Mir-188-3p targets skeletal endothelium coupling of angiogenesis and osteogenesis during ageing. *Cell Death Dis*. 2022;13(5):494. doi:10.1038/s41419-022-04902-w
45. Mohammed AA, Elsherbini AM, Ibrahim FM, El-Meadawy SM, Youssef JM. Biological effect of the nanocrystalline calcium sulfate bone graft in the periodontal regeneration. *J Oral Biol Craniofac Res*. 2021;11(1):47–52. doi:10.1016/j.jobcr.2020.10.012
46. von Hertzberg-Boelch SP, Luedemann M, Rudert M, Steinert AF. PMMA bone cement: antibiotic elution and mechanical properties in the context of clinical use. *Biomedicines*. 2022;10(8):1830. doi:10.3390/biomedicines10081830
47. van Vugt TAG, Geurts J, Arts JJ. Clinical application of antimicrobial bone graft substitute in osteomyelitis treatment: a systematic review of different bone graft substitutes available in clinical treatment of osteomyelitis. *BioMed Res Int*. 2016;2016:6984656. doi:10.1155/2016/6984656